# Absolute phase and amplitude mapping of surface acoustic wave fields

Damien Teyssieux, Thomas Baron, Jean-Michel Friedt \*, Gilles Martin and Pascal Vairac FEMTO-ST Institute UMR 6174

Université de Franche-Comté, CNRS, ENSMM, UTBM 32 Avenue de l'Observatoire, F-25044 Besançon, France

\* SENSeOR SAS, Besançon, France, hosted by FEMTO-ST

Abstract—This paper describes the development of a scanning heterodyne interferometer for acoustic wave energy mapping. A robust optical double pass interferometer setup is presented, allowing absolute phase and absolute magnitude measurements of the out-of-plane vibration component witin a 5 to 1200 MHz frequency range, only limited by the photodetector bandwidth. By using a dedicated high frequency demodulator, the system is insensitive to the low-frequency mechanical vibration. The system is here used on single-port Surface Acoustic Wave, allowing for the identification of energy distribution as a function of operating frequency and the acoustic velocity over the Bragg mirrors surrounding the resonator. We envision such an instrument as a tool for assessing acoustic energy confinement allowing for optimizing resonator quality factors aimed at providing improved frequency source stability.

#### I. Introduction

Acoustic wave propagation on piezoelectric material is well-known and has led to a thriving use in filters [1], resonators [2] and sensors [3]. While accurate design tools have been developed [4], rising operating frequencies emphasize some of the one dimensional or two-dimensional limitations of the models including the effect of the busses on acoustic energy guiding and more generally of energy confinement. Furthermore, actual manufacturing of high frequency devices reaches the technological limits of lithography and electrode patterning tool, yielding the need for experimental validation of the acoustic energy distribution in the device.

Acoustic energy mapping is a rich analysis method complementary to the classical electrical S-parameters characterization since the latter is insufficient for a good acoustic phenomena understanding. Consequently, several optical setups have been developed in order to measure the surface acoustic vibration, with an emphasis on mapping speed since the faster the characterization, the less prone the measurement is to environmental disturbances and most significantly temperature drift. While magnitude detection is readily achieved by using power measurement of the signal modulated by the acoustic wave in any interferometric strategy, sufficient for energy distribution mapping, the more subtle phase information needed to extract the phase velocity is more challenging due to the slow drift inherent to the high sensitivity to environmental parameters of interferometric setups. Indeed, the challenging aspect of the basic homodyne interferometric approach is its sensitivity to the static phase and hence the slow drift over time of this component which might be suppressed using postprocessing but is best eliminated using extended modulation approaches to get rid of this slowly static phase variation. Some of the classical solutions include the Sagnac interferometer proposed by Tachizaki et al. [5], also used by Hashimoto et al. [6], or another setups by Kokkonnen et al. [7], Martinussen et al. [8], Graebner et al. [9].

In this paper, an alternative approach is proposed, using amplitude splitting heterodyne interferometry. In a first part the theory justifying this concept is proposed, followed by a description of the experimental setup. Finally some results when scanning Surface Acoustic Wave (SAW) resonators operating at  $393\pm1$  MHz are presented.

# II. THEORY AND OPTICAL SETUP A. Amplitude splitting interferometry

Generally and for out-of-plane vibration measurement, amplitude splitting interferometry is used. The Michelson interferometer [10],[11] is the most common configuration. It is based on two arms corresponding to a splitting of a beam of light, with the first acting as a reference arm (fixed path) and the second as the signal arm (movable arm). Both beams are recombined to produce an interference pattern, assuming perfect alignment, resulting in a fringe pattern corresponding to the phase difference between the two waves. This phase difference is, assuming a quadrature condition, locally proportional to the optical path difference. In the case of a monochromatic source (e.g. laser beam), and because the frequency of light waves is too high to be detected by currently available detectors, the resulting intensity is proportional to:

$$I = I_o \left[ r_s + r_{ref} + 2\sqrt{r_s r_{ref}} \cos \left( \frac{4\pi \left( \Delta d - \Delta n \right)}{\lambda} \right) \right]$$
 (1)

where  $r_s$  and  $r_{ref}$  are the reference mirror and the sample reflectivity, respectively,  $\Delta d$  is the optical path difference due to the object movement,  $\Delta_n$  is the optical static phase difference between the sample and reference paths and  $\lambda$  is the wavelength of the laser. By assuming a sinusoidal out of plane surface vibration  $A\cos{(\omega t + \varphi)}$ , the resulting intensity is:

$$I(t) = I_c + 2I_o\sqrt{r_s r_{ref}}\cos\left(\frac{4\pi A}{\lambda}\cos(\omega t + \varphi) - \Phi_n\right)$$
 (2)

This equation corresponds to a homodyne interferometer and shows that the resulting intensity depends on the sample reflectivity.

When the vibration amplitude is small compared to  $\lambda$ , the Bessel development of the solution of eq. (2) is simplified

[12],[13] into:

$$I'(t) \propto \cos(\Phi_n) + \frac{4\pi A}{\lambda} \cos(\omega t + \varphi) \sin(\Phi_n)$$
 (3)

Several methods allow to stabilize the interferometer ( $\Phi_n$  =

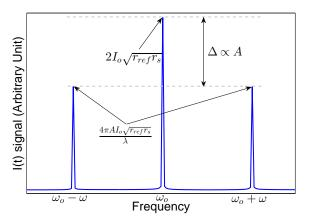


Fig. 1. Fourier Transform of the heterodyne interference signal.

 $(2n+1)\pi/2)$  in order to measure an absolute amplitude and an absolute phase [14] but at the cost of increasing the system complexity. At least one significant issue with the homodyne method concerns the radio frequency leakage. In order to suppress the sample reflectivity problem and diminish radio frequency leakage problems, a frequency shift can be introduced in one of the interferometer arms [7]. This frequency shifting can be achieved by using an Acousto-Optical Modulator (AOM). In this way, the resulting interference intensity, when the vibration amplitude is small compared to  $\lambda$ , is [15]:

$$I(t) = 2I_{o}\sqrt{r_{ref}r_{s}}\left[\cos\left(\omega_{o}t + \Phi_{n}\right) + \frac{2\pi A}{\lambda}\cos\left(\left(\omega_{o} + \omega\right)t + \varphi + \Phi_{n} - \frac{\pi}{2}\right) + \frac{2\pi A}{\lambda}\cos\left(\left(\omega_{o} - \omega\right)t - \varphi + \Phi_{n} - \frac{\pi}{2}\right)\right]$$
(4)

This equation corresponds to a heterodyne interferometer, where  $\omega_o$  corresponds to the AOM frequency shift, resulting in a signal of interest observed as a modulation peak  $(\omega_o)$  and two neighbouring peaks  $(\omega_o \pm \omega)$ . The theoretically absolute value of Fourier Transform of I(t) signal is shown in Fig.1. The absolute amplitude vibration is directly achieved by the modulation/neighbouring peak magnitude ratio (or decibel difference), independent to the sample surface reflectivity. By comparing the phases of the modulation and neighbouring peaks, the absolute phase of the surface vibration is obtained. Thus the static phase  $\Phi_n$  is suppressed.

Such an approach has been selected and the associated experimental setup is described in the next section.

## B. Optical setup description

The optical setup is based on a double-pass heterodyne interferometer [16]. A schematic of the interferometer is shown in Fig.2. The quarter-wave plate's (QWP) fast axis angle is adjusted at  $45^{\circ}$  with respect to the incoming beam linear polarization. After passing through the quarter-wave plate, the laser beam exhibits circular polarization. By passing through the Polarizing Beam Splitter (PBS), the beam is divided into

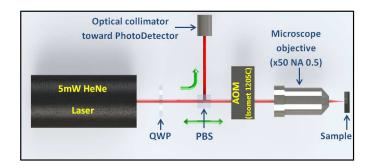


Fig. 2. Optical setup of the double-pass heterodyne interferometer (QWP: quarter-wave, plate PBS: polarizing beamsplitter and AOM: Acousto Optic Modulator)

two beams. The first beam (vertical polarization) is directed towards the optical fiber collimator, acting as the reference arm of the interferometer. The second beam (corresponding to the horizontal polarization) is directed trough the Acoustic Optical Modulator (AOM). The angle between the incident beam and the AOM is set in order to obtain the first diffraction order collinear to the laser beam (the zero order diffraction mode is not used). This beam is the signal arm of the interferometer. After reflection on the sample (by passing trough the microscope lens), the beam is phase modulated by the surface sample vibration and is directed again in the AOM and through the PBS. Due to the quarter-wave plate, the beam has a circular polarization. By using the reflexion on the laser mirror, the signal is directed towards the optical fiber collimator (vertical polarization) and interferes with the reference beam. Use of the mirror of the laser is not problematic (potentially yielding laser instability) in this case due to the frequency shift (AOM double-pass). When the vibration amplitude is small compared to  $\lambda$ , the interference signal of this setup is given by:

$$I(t) = 2I_{o}\sqrt{r_{ref}r_{s}}\left[\cos\left(2\omega_{o}t + \Phi_{n}\right) + \frac{2\pi A}{\lambda}\cos\left(\left(2\omega_{o} + \omega\right)t + \varphi + \Phi_{n} - \frac{\pi}{2}\right) + \frac{2\pi A}{\lambda}\cos\left(\left(2\omega_{o} - \omega\right)t - \varphi + \Phi_{n} - \frac{\pi}{2}\right)\right]$$
(5)

Eq. (5) emphasizes the two passes of the light beam through the AOM, yielding a  $2\omega_o$  term which will vanish during the demodulation process described in the next section.

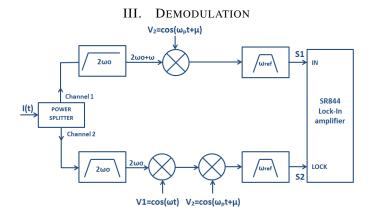


Fig. 3. Demodulation scheme: the recorded signal passing twice through the AOM is centered on a  $2\omega_o$  frequency which will be out of the analysis frequency range of  $S_1$  and  $S_2$ .  $\omega$  is the SAW device operating frequency.  $\omega_p$  is user selected through  $\omega_{ref}$  as defined in the text.

The setup of the electronic demodulation is schematically shown in Fig.3. S is the interference signal from the interferometer (eq.5),  $V_1$  is the sample drive signal and  $V_2$  is a new user defined signal (from another signal generator, Fig. 3) where  $\mu$  is the phase difference between  $V_1$  and  $V_2$ . With  $\omega_p = 2\omega_o + \omega - \omega_{ref}$  and after band-pass filtering at  $\omega_{ref}$ :

$$S_1 = \frac{I_o \sqrt{r_{ref} r_s} \pi A}{\lambda} \cos \left( \omega_{ref} t + \Phi_n - \mu - \frac{\pi}{2} + \varphi \right)$$
 (6)

$$S_2 = \frac{I_o \sqrt{r_{ref} r_s}}{4} \cos\left(\omega_{ref} t + \Phi_n - \mu - \frac{\pi}{2}\right) \tag{7}$$

 $S_1$  and  $S_2$  are detected synchronously by a RF lock-in amplifier (SR844 Stanford Research), where  $S_2$  is the lock signal. This setup allows for a maximum detection frequency of 4.5 GHz, limited by the operating bandwidth of the RF components.  $\omega_{ref}$  is set on the Lock-in frequency range (0-200 MHz for the SR844). This modulation scheme does not require the clocks of the two signal generators ( $V_1$  driving SAW and  $V_2$ ) since the drifting phase  $\mu$  between these two sources is discarded when mixing in the two branches of the demodulation scheme (Fig. 3).

#### IV. EXPERIMENT AND RESULTS

The objective of the experiments described in this section is to demonstrate the measurement of the acoustic amplitude as well as the acoustic phase of SAW devices, and more specifically a single port SAW resonator. This resonator is obtained by patterning aluminum electrodes using a lift-off process on AT-cut quartz. We select a metallization to period ratio a/p=0.5 and an acoustic period  $\lambda$  of 8  $\mu$ m. The single port resonator is constituted by one hundred interdigited electrodes in a comb layout, and one hundred Bragg reflectors acting as mirrors on each sides of the transducer. The frequency characterization using a network analyzer exhibits a strong resonance, which is well observed when measuring the acoustic vibration field at one point (Fig.4). In addition to the main resonance at 392.26 MHz, another mode at a nearby frequency is observed at 394.7MHz.

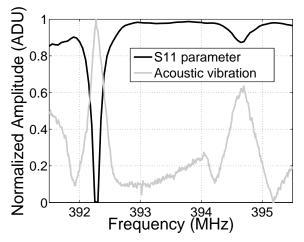


Fig. 4. Electrical reflection coefficient and single-position optical characterisation of the acoustic field magnitude of a single port reflective SAW resonator.

Based on the electrical measurement characteristics of this SAW device, optical mapping of the acoustic field characteristics is performed at both these frequencies. The result of the optical scan characterization on this resonator is shown

in Fig. 5 at (a) 392.26 MHz and (b) 394.7 MHz. On the main resonance at 392.26 MHz, the maximum amplitude is well characterized as a light-colored area located over the interdigitated comb transducers. For the second resonance at 394.7 MHz, the maximum amplitude exhibits the parasitic pattern due to the refraction of the acoustic waves under the electrode busses .

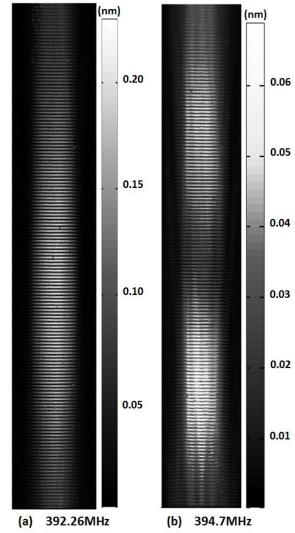


Fig. 5. Optical scan charactization of the acoustic field (out of plane component) amplitude of a single port resonator at (a) 392.26 MHz and (b) 394.7 MHz. Notice that the visual appearance of the stripes, associated with the acoustic nodes and antinodes, is associated due to aliasing of the image.

Following the optical scan characterization, phase information is extracted as shown in Fig.6. A zoom on several periods, which is possible thanks to the large size of the acoustic period and hence wide electrode spacing, exhibits the spatial distribution of the acoustic phase this device, with a  $2\pi$  rotation over one mechanical period. Unwrapping this acoustic phase information along the acoustic propagation direction provides an estimate of the acoustic velocity. As shown in Fig. 7, the propagating wave over each mirror (positions 0 to 1250 and 1330 to 2400  $\mu$ m) are characterized by acoustic propagation velocities of equal value but opposite sign (slope of the phase v.s distanc relationship), while the acoustic velocity cancels at the standing wave area over the acoustic cavity (positions 1250 to 1330  $\mu$ m). The observed acoustic velocity, obtained

by considering that the phase  $\varphi$  to position x slope is given by

$$\frac{d\varphi}{dx} = 2\pi \frac{f}{c} = \frac{2\pi}{\lambda} \Rightarrow c = 2\pi f \left(\frac{d\varphi}{dx}\right)^{-1}$$

of  $c=3138.7\pm1$  m/s on both slopes, is consistent with the SAW device operating frequency of  $c=\lambda\times f=8~\mu\mathrm{m}\times 392.26$  MHz=3138 m/s. The scanning probe measurement hence demonstrates the ability to characterize the acoustic propagation and confinement capabilities on a SAW resonator configuration, a requirement for experimentally assessing the main characteristics of a SAW design (acoustic velocity and reflection coefficient on the Bragg mirror electrodes) and understanding the cause for spurious modes or quality factor characterization beyond the basic electrical characteristics. Notice on the zoom of the slopes the ripples associated with the standing wave between adjacent interdigitated fingers. The periodicity of these ripples is 4  $\mu\mathrm{m}$ , consistent with a standing wave pattern between adjacent electrodes.

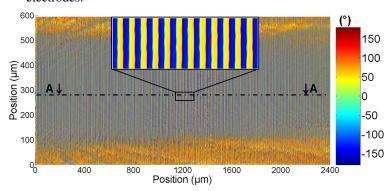


Fig. 6. Optical scan charactization of the acoustic field (out of plane component) phase of a single port resonator at 392.26 MHz.

#### V. CONCLUSION

Scanning probe mapping of the acoustic field charateristics, magnitude and most importantly phase, are demonstrated on radiofrequency surface acoustic wave devices using an amplitude splitting heterodyne interferometry approach. This method was selected for its stability and ease of optical alignment, while being insensitive to reflectivity and static phase variations as the scanning takes place. The measurement method, compatible with a use at acoustic device operating frequencies of up to 4.5 GHz, is demonstrated on a 392 MHz SAW resonator. The acoustic velocity of the wave propagating over the Bragg mirrors is observed as the slope of the unwrapped phase  $\nu$ s position map.

### ACKNOWLEDGMENT

This work was partly supported by the french RENATECH network and its FEMTO-ST technological facility. The authors thank the Ecole Nationale Supérieure de Mécanique et des Microtechniques (ENSMM) for funding support through the BQR grant and the Agence Nationale pour la Recherche through the Grant P2N 2010 'Phemto' . The authors also thanks Sébastien Euphrasie for his scientific suggestions.

#### REFERENCES

[1] C. Campbell, Surface Acoustic Wave Devices and Their Signal Processing Applications. Academic Press, 1989.

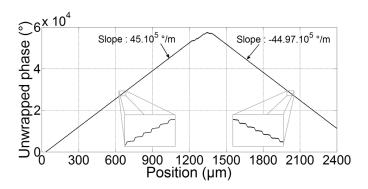


Fig. 7. Unwrapped phase along the AA cross section of Fig. 6: the acoustic cavity extends from positions 1250 to 1330  $\mu$ m and is surrounded by Bragg mirrors over which the acoustic wave propagates at a velocity related to the slope of the observed linear reltionship between phase and position. Inset: zoom on the phase evolution as a function of position, exhibiting the standing wave between interdigitated transducers.

- [2] G. Montress, T. Parker, and D. Andrea, "Review of SAW oscillator performance," in *Proc. IEEE Ultrasonics Symposium*, 1994, pp. 43–53.
- [3] D. Royer and E. Dieulesaint, *Elastic Waves in Solids, Vol. 2*. Springer, 2000.
- [4] S. Ballandras, R. Lardat, M. Wilm, T. Pastureaud, A. Reinhardt, N. Champavert, W. Steichen, W. Daniau, V. Laude, R. Armati, and G. Martin, "A mixed finite element/boundary element approach to simulate complex guided elastic wave periodic transducers," *Journal* of Applied Physics, vol. 105, p. 014911, 2009.
- [5] T. Tachizaki, T. Muroya, O. Matsuda, Y. Sugawara, D. Hurley, and O. Wright, "Scanning ultrafast sagnac interferometry for imaging twodimensional surface wave propagation," *Review of Scientific Instruments*, vol. 77, p. 043713, 2006.
- [6] K. Hashimoto, K. Kashiwa, N. Wu, T. Omori, M. Yamaguchi, O. Takano, S. Meguro, and K. Akahane, "A laser probe based on a sagnac interferometer with fast mechanical scan for RF surface and bulk acoustic wave devices," *IEEE Trans Ultrason Ferroelectr Freq* Control., vol. 58, no. 1, pp. 187–194, 2011.
- [7] K. Kokkonen and M. Kaivola, "Scanning heterodyne laser interferometer for phase-sensitive absoluteamplitude measurements of surface vibrations," *Appl. Phys. Lett.*, vol. 92, p. 063502, 2008.
- [8] H. Martinussen, A. Aksnes, and E. Engan, "Wide frequency range measurements of absolute phase and amplitude of vibrations in microand nanostructures by optical interferometry," *Opt. Express.*, vol. 15, no. 18, pp. 11370–11384, 2007.
- [9] J. E. Graebner, B. P. Barber, P. L. Gammel, D. S. Greywall, and S. Gopani, "Dynamic visualization of subangstrom high-frequency surface vibrations," *Appl. Phys. Lett.*, vol. 78, no. 2, pp. 159–161, 2001. [Online]. Available: http://link.aip.org/link/?APL/78/159/1
- [10] J. V. Knuuttila, P. T. Tikka, and M. M. Salomaa, "Dynamic visualization of subangstrom high-frequency surface vibrations," *Opt. Lett.*, vol. 25, no. 9, pp. 613–615, 2000.
- [11] J. Lawall and E. Kessler, "Michelson interferometry with 10 pm accuracy," Rev. Sci. Instrum., vol. 71, no. 7, pp. 2669–2676, 2000.
- [12] F. Larmer, A. Schilp, K. Funk, and C. Burrer, "Experimental characterization of dynamic micromechanical transducers," *J. Micromech. Microeng.*, vol. 6, pp. 177–186, 1996.
- [13] M. Abramowitz and I. Stegun, Handbook of Mathematical Functions with Formulas, Graphs, and Mathematical Tables. Dover Publications, 1964.
- [14] L. Lipiäinen, K. Kokkonen, and M. Kaivola, "Phase sensitive absolute amplitude detection of surface vibrations using homodyne interferometry without active stabilization," *J. Appl. Phys.*, vol. 108, p. 114510, 2010.
- [15] J. P. Monchalin, "Heterodyne interferometric laser probe to measure continuous ultrasonic displacements," *Rev. Sci. Instrum.*, vol. 56, no. 4, pp. 543–546, 1985.
- [16] P. Vairac and B. Cretin, "New structures for heterodyne interferometric probes using double-pass," optics communications, vol. 132, pp. 19–23, 1996.